

REPORT DOCUMENTATION PAGE

The public reporting burden for this collection of information is estimated to average 1 hour per response, including gathering and maintaining the data needed, and completing and reviewing the collection of information. Send comments information, including suggestions for reducing the burden, to Department of Defense, Washington Headquarters Service, 1215 Jefferson Davis Highway, Suite 1204, Arlington, VA 22202-4302. Respondents should be aware that notwithstanding any penalty for failing to comply with a collection of information if it does not display a currently valid OMB control number.
PLEASE DO NOT RETURN YOUR FORM TO THE ABOVE ADDRESS.

AFRL-SR-AR-TR-05-
0353

1. REPORT DATE (DD-MM-YYYY) 10-08-2005		2. REPORT TYPE Final Performance Report		DATES COVERED (From - To) 1 June 2002 - 31 May 2005	
4. TITLE AND SUBTITLE Sensitivity of Neurotransmitter Release to Radiofrequency Fields				5a. CONTRACT NUMBER	
				5b. GRANT NUMBER F49620-02-1-0306	
				5c. PROGRAM ELEMENT NUMBER	
6. AUTHOR(S) Craviso, Gale L. and Chatterjee, Indira				5d. PROJECT NUMBER	
				5e. TASK NUMBER	
				5f. WORK UNIT NUMBER	
7. PERFORMING ORGANIZATION NAME(S) AND ADDRESS(ES) University of Nevada, Reno Sponsored Projects, Mail Stop 325 204 Ross Hall Reno NV 89557-0240				8. PERFORMING ORGANIZATION REPORT NUMBER	
9. SPONSORING/MONITORING AGENCY NAME(S) AND ADDRESS(ES) USAF, AFRL AF Office of Scientific Research 875 North Randolph Street, Room 3112 Arlington VA 22203 <i>NE</i>				10. SPONSOR/MONITOR'S ACRONYM(S) AFOSR	
				11. SPONSOR/MONITOR'S REPORT NUMBER(S)	
12. DISTRIBUTION/AVAILABILITY STATEMENT Unlimited					
13. SUPPLEMENTARY NOTES					
14. ABSTRACT Exploring the interactions between radiofrequency (RF) radiation and biological systems is essential for developing RF-based non-lethal stunning/immobilizing weaponry. To this end a research effort was initiated to identify RF parameters potentially capable of selectively altering exocytosis, the process underlying neurotransmitter release and hence nervous system functioning. Major accomplishments included 1) designing, setting up, testing, characterizing and optimizing a waveguide-based RF exposure system for assessing effects on exocytosis, using neurosecretory adrenal chromaffin cells as an in vitro model, and 2) performing experiments that lead to the novel observation of enhanced neurosecretion in response to modulated RF fields in the 0.75 – 0.85 GHz frequency range. The research, which has been transitioned into the DoD EPSCoR program, has been presented at four international meetings, two local research conferences, and has culminated in one peer-reviewed publication, a manuscript in preparation and a Master's thesis.					
15. SUBJECT TERMS Radiofrequency fields, non-thermal bioeffects, waveguide-based radiofrequency exposure system, neurotransmitter release, adrenal chromaffin cells, FDTD numerical modeling					
16. SECURITY CLASSIFICATION OF:			17. LIMITATION OF ABSTRACT Unclassified Unlimited	18. NUMBER OF PAGES 11	19a. NAME OF RESPONSIBLE PERSON Gale L. Craviso
a. REPORT Unclassified	b. ABSTRACT Unclassified	c. THIS PAGE Unclassified			19b. TELEPHONE NUMBER (Include area code) 775-7784-4118

FINAL PERFORMANCE REPORT

Technical Proposal entitled: "Sensitivity of Neurotransmitter Release to Radiofrequency Fields"

Award Number: F49620-02-1-0306

Start Date: 01 June 2002

Termination Date: 31 May 2005

Interval for Final Performance Report: 01 June 2002 – 31 May 2005

Principal Investigator: Gale L. Craviso, Ph.D.
Associate Professor of Pharmacology
Dept. of Pharmacology
Howard Building, Room 219
University of Nevada School of Medicine
Reno, NV 89557
Phone: 775-784-4118
Fax: 775-784-1620
Email: gcraviso@unr.edu

20050901 077

ABSTRACT

Exploring the interactions between radiofrequency (RF) radiation and biological systems is essential for developing RF-based non-lethal stunning/immobilizing weaponry. To this end a research effort was initiated to identify RF parameters potentially capable of selectively altering exocytosis, the process underlying neurotransmitter release and hence nervous system functioning. Major accomplishments included 1) designing, setting up, testing, characterizing and optimizing a waveguide-based RF exposure system for assessing effects on exocytosis, using neurosecretory adrenal chromaffin cells as an *in vitro* model, and 2) performing experiments that lead to the novel observation of enhanced neurosecretion in response to modulated RF fields in the 0.75 – 0.85 GHz frequency range. The research has been presented at four international meetings, two local research conferences, and has culminated in one peer-reviewed publication, a manuscript in preparation and a Master's thesis. That aspect of our work specifically utilizing state-of-the art FDTD software has been featured on the website of Remcom, Inc. Personnel involved in the project, which included a neurobiologist and an electrical engineer as principal investigators, an associate engineer and two research assistants, provided a unique interdisciplinary research experience for both graduate and undergraduate students. The research has been transitioned into the DoD EPSCoR program.

SUMMARY

Objective:

To define radiofrequency (RF) parameters that produce non-thermal effects on catecholamine release, using bovine adrenal chromaffin cells as the *in vitro* model system and a cell perfusion system that allows us to monitor catecholamine release during RF exposure.

Accomplishments:

1. The design, set-up and testing of a waveguide-based RF exposure system for on-line monitoring of basal and stimulated catecholamine release from adrenal medullary chromaffin cells during RF exposures in the 0.75-1 GHz frequency range was completed. This included: 1) optimizing a cell perfusion apparatus for monitoring catecholamine release via electrochemical detection during RF exposure; 2) carrying out a detailed characterization of the RF exposure system using Finite-Difference Time-Domain (FDTD) numerical modeling, and optimizing the RF exposure system as dictated by the modeling results; 3) assembling a RF-generating system that would be capable of producing continuous wave, modulated and pulsed RF fields); 4) computer automation of all RF parameter protocols; 5) computer automation as well as measuring, data-logging and display of both temperature within the cell-perfusion apparatus and electrochemical output; 6) designing and optimizing a temperature feedback control system to maintain the cells at a constant temperature during RF exposure.
2. A series of experiments were carried out in a waveguide that was either terminated in a short or terminated in a matched load. These experiments spanned the 0.75 – 1 GHz frequency range and included continuous wave, amplitude modulated and pulse modulated RF fields for the exposures.

New Findings:

The primary finding of our experiments is an apparent increase in nicotinic receptor-stimulated catecholamine release in the presence of 20 Hz amplitude-modulated as well as pulsed RF fields in the 750 – 850 MHz frequency range. Gross heating does not appear to be the mechanism underlying the effect. These data are being prepared for publication.

Publications:

Hagan, T., Chatterjee, I., McPherson, D. and Craviso, G.L. "A novel waveguide-based radiofrequency/microwave exposure system for studying non-thermal effects on neurotransmitter release - Finite-Difference Time-Domain modeling". IEEE Transactions on Plasma Science 32: 1668-1676, 2004.

Thesis:

Todd Hagan, completed his M.S. in Electrical Engineering at the University of Nevada, Reno in May 2005; his thesis is titled: "Finite-Difference Time-Domain modeling of a waveguide-based radiofrequency exposure system for studying non-thermal effects on catecholamine release from chromaffin cells". Todd is continuing to work toward a Ph.D. in Electrical Engineering.

Interactions/Transitions:

a) Presentations

i) Oral Presentations:

Hagan, T., Chatterjee, I., McPherson, D. and Craviso, G.L. "Finite-Difference Time-Domain modeling of a waveguide-based radiofrequency exposure system for studying non-thermal effects on catecholamine release from chromaffin cells". 3rd International Symposium on Nonthermal Medical/Biological Treatments using Electromagnetic Fields and Ionized Gases (ElectroMed 2003), San Antonio, TX, June 2003.

Craviso, G.L., Brouse, D., Hagan, T., McPherson, D. and Chatterjee, I. "Effect of radiofrequency electromagnetic fields on catecholamine release from cultured bovine adrenal chromaffin cells". Selected presentation at the "Hot Topics" session of the Gordon Research Conference on Bioelectrochemistry, New London, CT, July 2004.

ii) Poster Presentations

National/International:

Hassan, N., Chatterjee, I., Publicover, N.G., and Craviso, G.L. "A combined experimental and computational analysis of membrane potential variation in excitable cells in response to DC electric fields" at the CEIDP/IEEE meeting in Cancun, Mexico in October, 2002.

Craviso, G.L., Brouse, D., Hagan, T., McPherson, D. and Chatterjee, I. "Effect of radiofrequency electromagnetic fields on catecholamine release from cultured bovine adrenal chromaffin cells". Gordon Research Conference on Bioelectrochemistry, New London, CT, July 2004.

Craviso, G.L., Brouse D., Hagan, T., McPherson, D. and Chatterjee, I. "Investigations into non-thermal radiofrequency effects on the release of catecholamines from adrenal chromaffin cells". 4th International Symposium on Nonthermal Medical/Biological Treatments using Electromagnetic Fields and Ionized Gases (ElectroMed 2005), Portland, OR, May 2005.

Local:

Dipti Bhakta. "Optimizing and Characterizing an On-line Monitoring System to Measure Catecholamine Release from Bovine Adrenal Chromaffin cells during Radio-frequency (RF) Field Exposure", presented to the University of Nevada research community at the Desert Research Institute, Reno, NV August 8, 2002.

Chaithra Prasad. "Quantification of catecholamine levels in cultured bovine adrenal chromaffin cells", presented to the University of Nevada, Reno, Biochemistry Research program at the School of Medicine, Reno, NV, May 4, 2005.

b) Consultative and advisory functions: None

c) Transitions – DoD EPSCoR program, Award No. F49620-03-1-0262

New Discoveries, inventions or patent disclosures: None

Honors/Awards: Hagan et al., 2004, is featured on the website for Remcom, Inc., the company that developed the XFDTD software package used in our numerical modeling studies.

Personnel involved in the project

Gale L. Craviso, Ph.D., Associate Professor of Pharmacology – Principal Investigator
Indira Chatterjee, Ph.D., Professor of Electrical Engineering – Co-Principal Investigator
Dana McPherson, Associate Engineer, Dept. of Electrical Engineering
Mike Trakas, Research Assistant
David Brouse, Research Assistant
Todd Hagan, M.S. graduate student in Electrical Engineering
Dipti Bhakta, undergraduate junior student in Mechanical Engineering
Chaithra Prasad, undergraduate senior student in Biochemistry

COMPREHENSIVE TECHNICAL SUMMARY

Rationale

The United States Department of Defense is one of the world's largest developers and users of RF-emitting systems for radar, communication and anti-electronic weaponry purposes. However, the use of RF radiation as a non-lethal weapon *per se* has not yet been realized, most likely because the effects of exposure of biological systems to RF fields at levels that do not produce thermal effects are largely unknown. The overall objective of the research funded by this grant was to begin laying the foundation upon which RF technology can be developed that would have an application for non-lethal weaponry purposes, such as stunning/immobilizing the enemy. To accomplish this goal, we initiated a carefully designed and controlled investigation of the RF exposure parameters that can alter exocytosis, the process underlying neurotransmitter release. All experiments were carried out using a well-characterized model for studying exocytosis, isolated adrenal medullary chromaffin cells. These cells synthesize, store and release the catecholamines epinephrine and norepinephrine.

Experimental Procedure

1. RF Exposure System – Design and Construction

Because the identification of a true biological outcome, i.e., an effect on catecholamine release, requires uniform RF fields and known specific absorption rates (SAR), this necessitated our designing, constructing, characterizing and optimizing an RF exposure system that allows maximum flexibility in choosing the most common RF exposure parameters (e.g., frequency, modulation schemes, pulsing schemes, etc.) for experiments as well as permits optimal handling of cell samples under the constraints and limitations imposed by the biological experiment. In our particular case, the goal was on-line measurement of catecholamine release by electrochemical detection from perfused chromaffin cells during RF exposure. A waveguide-based exposure system was determined as being the most suitable one for our experimental needs.

A schematic diagram of the overall experimental setup is shown in Figure 1.

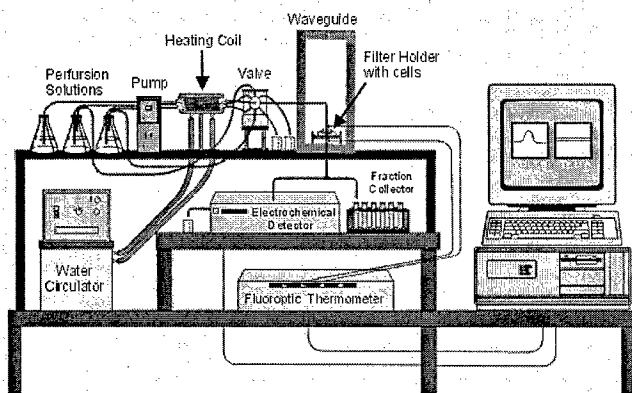


Figure 1. Chromaffin cells are loaded onto a GF/C glass fiber filter placed within a plastic filter holder and continuously superfused with temperature-controlled (36.5°C) balanced salt solution (BSS). Part of the effluent flows into an electrochemical detector (ECD) that measures on-line in the amperometric mode the amount of catecholamine released; the remaining effluent goes to a fraction collector for quantification of epinephrine and norepinephrine by high performance liquid chromatography. A computer-interfaced valve switches to a drug-containing BSS for stimulating catecholamine release with the nicotinic receptor agonist, dimethylphenylpiperazinium (DMPP). The cell perfusion apparatus is placed inside a waveguide for RF exposure.

Figure 2 below is a photograph of the actual cell perfusion system within the waveguide.

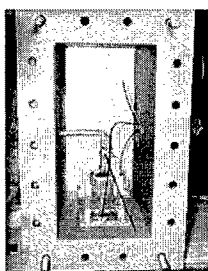


Figure 2. A standard WR 975 waveguide is used for exposing the cells to RF fields in the 0.75 – 1 GHz frequency. It is constructed out of aluminum and has undergone a chromate conversion process to prevent corrosion. It is equipped with several rectangular non-radiating slots (2.54 cm x 0.95 cm) at the top, bottom, and sides through which perfusion tubing and temperature probes gain access. Fluoroptic temperature probes continuously monitor the temperature of the BSS entering and exiting the filter holder and a temperature feedback system controls the flow of forced air blowing onto the BSS inlet tubing to maintain the temperature of the BSS superfusing the cells at 36.5°C during RF exposure. A third fluoroptic probe continuously monitors temperature inside the waveguide.

Experiments were carried out with the cells placed at the location of a standing wave magnetic or electric field maximum in the waveguide terminated by a short circuit as well as with the cells exposed to a traveling wave RF field when the waveguide was terminated in a matched load. Because effects of RF exposure on catecholamine release to date have only been observed using the waveguide terminated in a matched load (see Experimental Results section), a schematic diagram of this configuration only is presented (Figure 3).

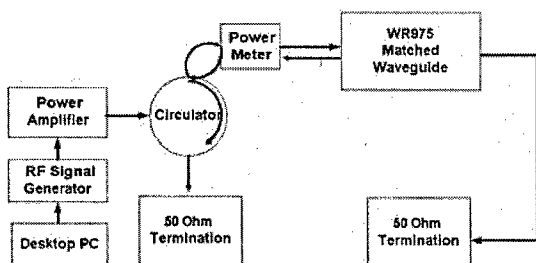


Figure 3. The signal generator (Agilent 8648B) generates the RF signal that is amplified (Instruments for Industry SMV 300 Solid State Amplifier) to the required input power. A circulator (UTE Microwave Inc. CT-1541N) is inserted in the circuit so that the reflected power is directed to a 50 Ω RF coaxial termination (Bird 300-ST). The power into the waveguide system is monitored by a power meter (Agilent E4416A) with a power sensor (Agilent E9325A), and coupled into the exposed waveguide via a coax-waveguide adapter.

A photograph of the actual RF exposure/experimental setup is shown in Figure 4.



Figure 4. All equipment has been interfaced with a computer using programs written in LabView. In addition, all RF parameter protocols are fully automated. Also, the experimental setup is computer automated for measuring, data-logging and display of temperature within the cell-perfusion apparatus as well as the ECD output.

2. RF Exposure System – Characterization and Optimization

The shorted waveguide RF exposure system was characterized and optimized using the FDTD numerical modeling technique. Complete details are given in Hagan et al., 2004. A detailed model of the cell perfusion apparatus inside the waveguide was constructed using the CAD software SolidWorks which was then imported into the commercially available FDTD software package XFDTD (BioPro Version 5.3, Remcom, Inc., State College, PA). The model took into account the precise geometries and dielectric properties of each component of the exposure system. Calculations of the electromagnetic fields and the distribution of the SAR in the region where the chromaffin cells are located were thus obtained and simulations allowed us to design exposure protocols that provided the most homogeneous SAR (typically, a standard deviation of inhomogeneity of less than $\pm 30\%$ is acceptable) over the region containing the cells.

The matched waveguide exposure system has been similarly modeled and figures provided in the Appendix show the distribution of the SAR and electric field, respectively, at the location of the cells exposed to 750 MHz fields.

Experimental Results

Initial experiments used a shorted waveguide where chromaffin cells were positioned in the electric field or magnetic field maximum of a standing wave at specific frequencies in the 0.75-1 GHz frequency range. None of the experiments showed effects on either basal or nicotinic receptor-stimulated catecholamine release during RF exposure, perhaps because the magnitude of the electromagnetic fields was not sufficiently high enough to elicit a response. To give us greater flexibility in exposure paradigms during a single experiment (e.g., the ability to expose cells to a multitude of frequencies), we switched to a matched waveguide, which meant that the cells would be exposed to traveling waves. At the same time, we substantially modified the cooling system for controlling and maintaining temperature within the physiological range of 36°-37C° so that the amount of power delivered into the waveguide could be increased without causing heating of the cells.

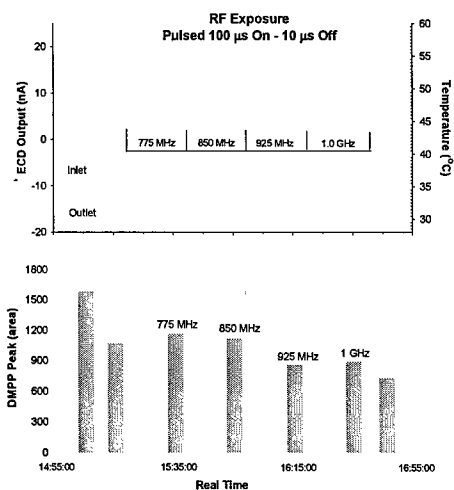
Using the matched waveguide exposure setup, an increase in nicotinic receptor-stimulated catecholamine release was observed during RF exposure of the cells to either pulsed or amplitude-modulated RF fields in the 750 – 850 MHz frequency range. Data from a representative experiment are shown in the Appendix. (Also provided in the Appendix is a table summarizing all the RF exposure parameters that have resulted in apparent effects on nicotinic receptor-stimulation of catecholamine release). No effects have been observed to date when the RF field was applied as a continuous wave or when higher frequencies were employed (0.85 – 1 GHz).

The effects on stimulated catecholamine release observed so far do not appear to be due to gross heating. First, there are no noticeable increases in temperature during the exposures that could account for the effects. Second, data from preliminary experiments indicate that the changes in nicotinic receptor-stimulated catecholamine release observed during RF exposure are not consistent with how increases in temperature alter nicotinic receptor-stimulated catecholamine release. That is, imposed temperature changes of up to 2°C failed to mimic the effects of RF exposure on nicotinic receptor-stimulated catecholamine release (see Appendix).

Ongoing work/future directions

Because the research funded by this grant has been transitioned into the DoD EPSCoR program, we are actively continuing experiments to further evaluate effects of RF fields on catecholamine release, employing a wider frequency range, additional pulsing paradigms and RF exposure protocols. Moreover, we are trying to develop strategies for delivering more power during RF exposures without causing gross heating. This will enable us to observe more robust and consistent effects. Finally, in an attempt to differentiate better between thermal and non-thermal effects of RF exposure on catecholamine release, we have begun devising a way to carry out a detailed investigation of how imposing rapid temperature changes on chromaffin cells affects catecholamine release.

APPENDIX

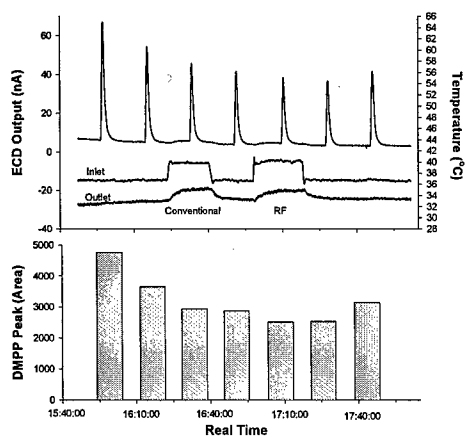


Representative experiment showing that RF exposure at 775 MHz and 850 MHz increases catecholamine release stimulated by the nicotinic receptor agonist DMPP. (Top) ECD profile showing stimulated catecholamine release with time in response to successive 30 second pulses of 5 μM DMPP. In the absence of RF exposure the amount released typically declines with each successive DMPP pulse. In the experiment shown here, two initial responses to DMPP were obtained and the cells then exposed to pulsed RF fields at 4 discrete frequencies (20 minute exposures). (Bottom) Area under the ECD curve for DMPP-stimulated catecholamine release. Inlet and Outlet refer to the temperature of the BSS entering and exiting the filter holder.

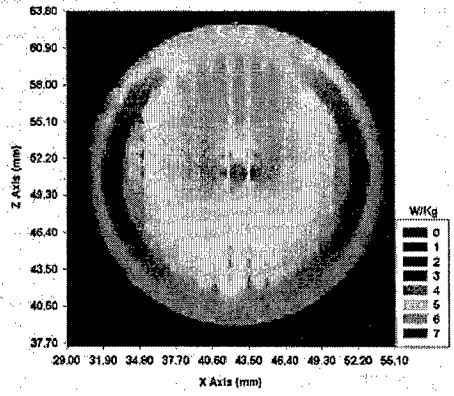
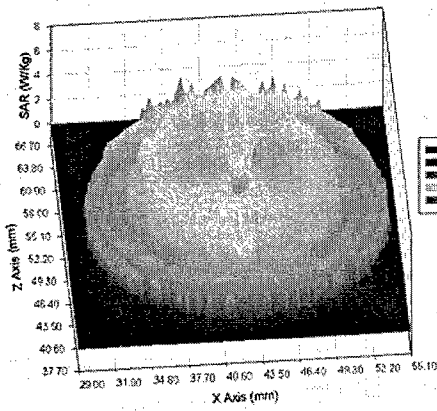
SUMMARY OF THE RF EXPOSURE CONDITIONS IDENTIFIED TO DATE IN WHICH AN INCREASED RESPONSE TO DMPP HAS BEEN OBSERVED

Frequency (GHz)	Type of Modulation	Avg. Power (W)	Peak Power (W)	SAR over 50% of the GF/C filter (W/kg)
0.750	AM (20 Hz square wave)	1.5	—	5 - 6
0.775 and 0.850	Pulse keying (100 μ s on, 10 μ s off, 9.1 kHz PRF)	2.27	2.5	7 - 10 (0.775) 7 - 9 (0.850)
0.750 and 0.800	Pulse keying (20 ns on, 215-180 ns off, 4.24 - 5 MHz PRF)	33.7 - 81.3	398 - 813	1300 - 1800 (0.75) 2200 - 3100 (0.8)
0.750	Pulse keying (20 ns on, 202 ns off, 4.5 MHz PRF)	61.4	724	2000 - 3000

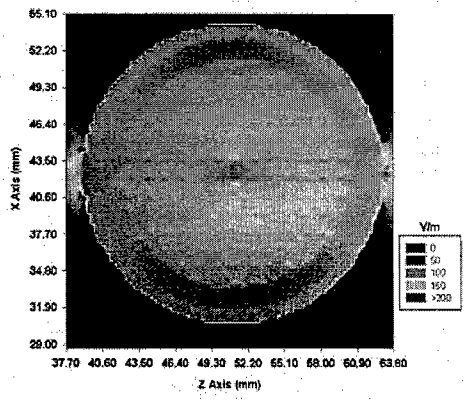
AM: amplitude modulation
PRF: pulse repetition frequency



Representative experiment showing that DMPP-stimulated catecholamine release does not increase when temperature rises. Temperature was elevated both by conventional heating (increasing the temperature of the BSS) or more rapidly by applying a 750 MHz continuous wave RF field at a power level that causes an overt rise in temperature of the BSS superfusing the cells.



Magnitude and distribution of the SAR (W/kg) on the glass fiber filter computed by XFDTD at 750 MHz for the matched waveguide. Contour plot (left) and surface plot (right).



Surface plot of the magnitude and distribution of the electric field (V/m) on the glass fiber filter computed by XFDTD at 750 MHz for the matched waveguide.

University of Nevada, Reno

**Finite-Difference Time-Domain Modeling of a Waveguide-Based
Radiofrequency Exposure System for Studying Non-Thermal Effects
on Catecholamine Release from Chromaffin Cells**

Characterization and Optimization

A thesis submitted in partial fulfillment of the requirements for the degree of Master of
Science in Electrical Engineering

By

Todd Hagan

Dr. Indira Chatterjee/ Dissertation Advisor

Dr. Gale Craviso/Dissertation Co-Advisor

April, 2005

Abstract

The scope of this thesis is two-fold. (1) To optimize the waveguide exposure system incorporating a cell perfusion apparatus (CPA) so as to provide maximum homogeneity of the electromagnetic fields (EMF) and specific absorption rate (SAR) in the region containing the biological cells. (2) To provide a detailed characterization of the EMF and SAR at the location of the cells. These two goals were achieved via numerical FDTD modeling. Macroscopic modeling was performed where the minimum Yee cell size used in the FDTD model was a fraction of a millimeter, representing accurately the waveguide and CPA physical structures. Preliminary microscopic modeling was also accomplished where the minimum Yee cell size was on the order of 0.1 μm , making it possible to take into account the basic morphological features of bovine adrenal medullar chromaffin cells used in the RF/MW exposure experiments.

The FDTD macroscopic modeling determined that the EMF and SAR spatial distribution, and hence the degree of homogeneity, across the location of the cells was dependent on the dielectric properties of the glass fiber filter (GFF) soaked with balanced salt solution (BSS) on which the cells were loaded, the geometry of the center BSS flow channel, the spatial distribution of cell loading onto the GFF, and how the EMF coupled (tangential or perpendicular) into the GFF. The direction of the incident electric field intensity (\vec{E}) must be tangential to the top and bottom of the GFF for maximum coupling to the cells. If the waveguide is terminated by a short with the CPA at the maxima of the resulting standing wave or if the waveguide was terminated by a matched load, the

degree of homogeneity was independent of input power and frequency of the RF/MW signal supplied to the exposure system. Also, with greater power, the amplitude of \vec{E} was larger across the location of cells, but retained the same spatial distribution.

Because the cell distribution is known after an actual exposure system by staining the GFF with the dye neutral red and the inputs into the FDTD model are the same RF parameters (i.e., power, modulation, frequency, etc.) as used in the experiment, the simulated EMF (or SAR) and cell spatial distributions could be overlaid to assist in interpreting the experimental results. Furthermore, with this knowledge, steps were taken to modify the CPA, e.g., tapering of the central BSS flow channel, to improve both the degree of field homogeneity and the efficiency of EMF coupling across the location the cells.

Preliminary FDTD microscopic modeling of a single cell and a linear cluster of three cells showed that the location of the maxima of the \vec{E} field inside and surrounding the cell were always at the plasma membrane. These maxima are at both the top and bottom of the cell with respect to the direction of the incident \vec{E} field, which is consistent with Raleigh scattering from a dielectric sphere. The spatial locations of the maxima are independent of amplitude and frequency. Very close proximity of cells, as in a cluster, resulted in nearly doubling the magnitude of \vec{E} in the region between the cells.

Subsequent spectral analysis of the microscopic simulations, however, indicated that although the greatest maxima occurred at the cell membrane for an incident Gaussian pulse waveform, different regions of a cell or cluster will couple different frequencies of the incident EMF with different efficiencies. In the frequency domain, the energy at a particular point in the cell will maximize at a particular frequency. The cell membrane

couples higher frequencies while regions away from the membrane and well within the cytoplasm couples low frequencies. This suggests that different regions of a cell could be targeted for greater exposure by simply changing the frequency, pulse width, or EMF incident waveform.

Acknowledgements

I wish to express my sincerest appreciation of Dr. Indira Chatterjee and Dr. Gale Craviso for giving me, a difficult student at the best of times, the chance to work on a fascinating project and in so doing allow my fledging engineering skills and analytical thinking and hence problem solving to find a firm foundation. These tools will forever be with me no matter what challenges I will encounter in the future.

I would also like to express much appreciation to Dana McPherson for his insightful yet down to earth pragmatism in directing my approach for overcoming serious technical issues both in software and hardware. His fabrication skills and valuable time were indispensable. But most of all, I want to thank him for the time when I worked under him as a student worker while earning my B.S. in electrical engineering. What I learned from him could never be acquired from classes or books, but only from a demonstration of knowledge gained from an affinity with engineering not unlike a master craftsman or artist has with their medium of creation.

Next, I would like to thank David Brouse for his crucial input and collaboration even if we would at times argue and beat each other over the head about the best way to solve or address a technical problem or issue. Our collaboration though sometimes loud resulted in immense improvements in the performance of the RF/MW exposure system and experiments.

I wish also to acknowledge Bindya Dumpala; her valuable insight and ability to pick up and discuss complicated programming issues in LabView helped me many times

to discover the needed crux or path to resolve any issue in an elegant and timely manner.

But most of all, I appreciate her as my best friend.

Finally but not at all least, I would like to convey my thanks to the United States Air Force Office of Scientific Research (AFOSR) for providing the financial support without which this project would not have been possible.

Table of Contents

• Dissertation Abstract	ii
• Acknowledgements	v
• Table Of Contents	vii
• List Of Figures	xi
• List Of Tables	xxii
Chapter 1	
Introduction	1
References	7
Chapter 2	
A novel waveguide-based radio frequency/microwave exposure system for studying non-thermal effects on neurotransmitter release Finite- difference time-domain modeling	
Abstract	12
I. Introduction	13
II. Methodology	
A. Cell Perfusion Chamber	14
B. Waveguide Exposure Set-up	18
C. FDTD Modeling of the Exposure System	20
D. Dielectric Properties of Materials Used in the Exposure System	25
III. Results and	
A. Model Validation	27

Discussion		
	B. Characterization of the RF Exposure System	31
	B.1.SAR Distribution with the Cell Perfusion Chamber at the Maximum in B	32
	B.1.a Perpendicular Orientation	32
	B.1.b Parallel Orientation	35
	B.2 SAR Distribution with the Cell Perfusion Chamber at the E field Maximum	35
	B.2.a Perpendicular Orientation	35
	B.2.b Parallel Orientation	36
IV. Conclusion		38
References		39
Chapter 3	Matched waveguide configuration of RF/MW exposure System: Characterization and Optimization	
	I. Introduction	44
	II. Methodology	
	A. Determining the optimum position of the CPA within the waveguide	50
	B. Improvements in the control of the temperature of BSS superfusing the cells	50
	C. Setting up the Matched waveguide	55
	D. Description of and Improvements in the FDTD Modeling of the Exposure System	56
	E. Dielectric Properties of Materials Used in the Exposure System	63

III. Results and Discussion	A. Model Validation	64
	B. Characterization of the RF Exposure System	65
	B.1 SAR distribution across a GFF that contains no cells	70
	B.2 SAR distribution across a GFF with evenly distributed cells	71
	B.3 SAR distribution across a GFF with cells concentrated in the middle of the filter	76
IV. Conclusion		80
References		81
Chapter 4	Determination of Dielectric Properties of materials comprising the RF/MW Exposure System	
	I. Introduction	83
	II. Methodology	
	A. Determination of the inherent error in the dielectric measurements	84
	B. Determination of the minimum sample thickness for low and high loss materials	87
	C. Drude model of BSS and BSS soaked filter	89
III. Results and Discussion	A. Dielectric permittivity for Low loss materials comprising the CPA	94
	B. Dielectric permittivity measurements for high loss materials and Drude model comparison	95
	C. Cell Loading: Its effect on the dielectric	

	properties of BSS soaked GFF	99
IV. Conclusion		104
References		107
Chapter 5	FDTD EM model of a bovine adrenal chromaffin cell and cell cluster immersed in 36°C BSS	
I. Introduction		110
II. Methodology	A. Model	111
	A.1 Geometry	111
	A.2 Dielectric Spectra	113
	A.3 Cell Cluster	121
	B. Excitation Waveform	122
	C. Post Analysis Software	124
	A. Single Cell Model	
III. Results and Discussion		
	A.1 The effects of short versus long pulse width	124
	A.2 Targeting specific regions of the cell	129
	B. Cluster of three cells	129
IV. Conclusion		132
References		133

List of Figures:

Figure 2.1	A. The RF/MW exposure system for experiments conducted at the E field maximum of the standing wave pattern	15
	B. A close up of the cell perfusion apparatus	16
Figure 2.2	Computer generated drawing of the cell perfusion apparatus	17
Figure 2.3	Computer generated drawing of the experimental setup being used for exposures	
	A. The B maximum of the standing wave pattern	19
	B. the E field maximum of the standing wave pattern	19
Figure 2.4	XFDTD model (numerical mesh) of the entire RF/MW exposure system with the cell perfusion apparatus positioned at the \vec{E} field maximum of the standing wave pattern for a frequency of 1.0 GHz	
	A. The yz plane	21
	B. The xy plane	22
Figure 2.5	Close up view of the XFDTD mesh (subgrid) for the cell perfusion apparatus at the \vec{E} field maximum of the standing wave. The mesh is composed of Yee cells with a side length of 0.3048 mm	

	A. Center cross-sectional view.	23
	B. 3D perspective view	23
Figure 2.6	Surface plots of the \vec{E} field and \vec{B}	
	A. based on waveguide theory using measured forward and reflected powers	30
	B. predicted by XFDTD model. Forward Power = 0.5 W, Frequency = 1 GHz.	30
Figure 2.7	A. Contour	33
	B. surface plot of the SAR distribution across the glass fiber filter (location of chromaffin cells) computed by XFDTD for the perpendicular orientation. The cell perfusion apparatus is at the maximum in \vec{B} of the standing wave pattern. Forward Power = 0.5 W, Frequency = 1.0 GHz.	34
Figure 2.8	A. Contour plot	37
	B. Surface plot of the SAR distribution across the glass fiber filter (location of chromaffin cells) computed by XFDTD for the parallel orientation. The cell perfusion apparatus is at the \vec{E} field maximum. Forward Power = 0.5 W, Frequency = 1.0 GHz	38
Figure 3.1	A. The RF/MW exposure system using a matched WR975 rectangular waveguide positioned with the longer dimension vertical in order to provide for	

	maximum coupling of \vec{E} field into the region containing the chromaffin cells	46
	B. Close up views of the CPA from the side.	47
	C. Close up views of the CPA from the top	48
Figure 3.2	The entire RF/MW exposure system in the matched waveguide configuration. Refrigerated air is forced over the inlet glass tubing at high but controlled velocities through the air conduit. The air is then exhausted out at the other side of waveguide.	51
Figure 3.3	A. An exploded view of the entire RF/MW exposure system	52
	B. a close up view of the CPA	52
	C. the GFF sandwiched between two 350 μm meshes. The column of BSS above and below the GFF is also depicted	52
Figure 3.4	Close up view of the modified CPA with the silicone rubber inlet tubing of chapter 2 replaced with a Pyrex TM glass tube. (XFDTD TM software 3D view after importing from Solid Works TM)	54
Figure 3.5	A. XFDTD 3D numerical mesh of the RF/MW exposure system	57
	B. a close-up view of the CPA. The left side of the waveguide is intentionally hidden for viewing purposes	58
	C. Center cross-section of this numerical mesh	59
	D. A close up-view of the CPA showing the measured temperatures observed in exposure experiments and on which the respective dielectric properties used in	

the FDTD model were based. 60

- Figure 3.6 The \vec{E} field distribution inside the waveguide without the CPA present calculated from standard waveguide theory for a power level of 0.5 Watts at 1 GHz
- A. Contour Plot 66
- B. Surface Plot 67
- Figure 3.7 A. Contour 68
- B. Surface Plots of the \vec{E} field magnitude computed without the CPA present in the XFDTD model. Graphed using Sigma Plot 69
- Figure 3.8 The spatial distribution of the SAR for the center plane of the GFF with no chromaffin cells loaded
- A. Contour Plot with the corresponding \vec{E} field and time rate change in temperature calculated based on a mass density of 1887.42 Kg/m^3 , effective electrical conductivity of 2.025 S/m , and a specific heat of $4082 \text{ JKg}^{-1}\text{C}^{-1}$ 72
- B. Surface Plot 73
- Figure 3.9 The spatial distribution of the SAR for the bottom plane of the GFF with no chromaffin cells loaded
- A. Contour Plot with the corresponding \vec{E} field and time rate of change in temperature calculated based on a mass density of 1887.42 Kg/m^3 , effective

electrical conductivity of 2.025 S/m, and a specific heat of $4082 \text{ JKg}^{-1}\text{C}^{-1}$

B. Surface Plot 75

Figure 3.10 The SAR magnitude spatial distribution for the center plane of the GFF when 4 million cells are loaded in a small cylindrical volume of 22.1 mm^3 at the center of GFF

A. Contour plot 77

B. Surface plot 78

Figure 4.1 Calibration of the network analyzer and dielectric probe by

A. measuring and then comparing to the theoretical complex permittivity of water at 25°C . 83

B. The percent difference between the measured and theoretical permittivities of water giving the percent error in dielectric measurements. 85

Figure 4.2 A. Narrow band measurements of the complex permittivity of BSS soaked GFF filters stacked in increments of 2 on a Styrofoam platform 88

B. The mean permittivity vs. number of stacked filters over the frequency band of 0.5 to 1.5 GHz. 88

Figure 4.3 A. Narrow band permittivity measurements of red dental putty to establish the minimum sample thickness 90

B. Convergence of the mean relative permittivity of samples supported by

	Styrofoam and metal over the frequency band of 0.5 to 1.5 MHz.	90
Figure 4.4	A. Setup for obtaining the BSS conductivity measurements	92
	B. Measured Conductivity vs. temperature of BSS.	92
Figure 4.5	Measured broadband dielectric permittivity of 55 stacked dry glass fiber filters	93
Figure 4.6	Broadband dielectric measurements of low loss materials comprising the CPA.	95
Figure 4.7	The complex dielectric spectra measured by the network analyzer and dielectric probe kit for	
	A. BSS	96
	B. BSS soaked GFF at the two extreme temperatures possibly encountered in the experiments.	96
Figure 4.8	The measured and theoretical dielectric spectra for BSS at the temperature typically occurring at the inlet	
	A. 37 °C and outlet	97
	B. 33 °C during experiments. These data are used in the XFDTD model of the RF/MW exposure system	97
Figure 4.9	The measured and theoretical dielectric spectra for BSS soaked GFF at the temperature of 36 °C that exposure experiments are conducted at. These data are used in the XFDTD model of the RF/MW exposure system.	98

Figure 4.10	<p>A. The calculated complex dielectric spectra based on Maxwell-Wagner theory at 36 °C for the GFF plus 4 million cells and compared to that of just GFF</p> <p>B. The percent difference of the real and imaginary components between GFF plus cells and just GFF.</p>	<p>102</p> <p>102</p>
Figure 4.11	<p>Two typical cell distributions on the GFF determined by staining the GFF with red neutral dye after RF/MW exposure experiments</p> <p>A. Cells are distributed throughout the available volume</p> <p>B. the cells are highly localized forming a LHM, a region of high cell concentration.</p>	<p>103</p> <p>103</p>
Figure 4.12	<p>The Maxwell-Wagner theoretical calculation of the dielectric properties for the BSS soaked GFF plus 4 million cells and just BSS soaked GFF for different cell loadings forming LHMs with increasing fractional volume, p</p>	<p>105</p>
Figure 4.13	<p>Percent difference in the dielectric properties</p> <p>A. Real Component</p> <p>B. Imaginary component, of the BSS soaked GFF plus 4 million cells and just BSS soaked GFF for different cell loadings forming LHMs with increasing fractional volume, p.</p>	<p>106</p> <p>106</p>
Figure 5.1	<p>A. XFDTD 3D transparent view of a chromaffin cell with nucleus in 36 °C BSS.</p> <p>B. center-cross section of XFDTD 3D numerical mesh with labeled points of interest.</p>	<p>113</p> <p>113</p>

Figure 5.2	Dielectric spectra of the B cell and the calculated chromaffin cell cytoplasm based on the Drude material parameters listed in Table I	119
Figure 5.3	Chromaffin cell cytoplasm dielectric spectra calculated based on Maxwell-Wagner mixture theory and the corresponding best fit Drude model	119
Figure 5.4	The percent difference verses frequency between the complex relative permittivity of the calculated chromaffin cell and that of the best fit Drude model	120
Figure 5.5	The complex relative permittivity of nucleoplasm in a chromaffin cell based on Table I parameters	120
Figure 5.6	XFDTD 3D model of a linear cluster of three cells immersed in 36°C BSS	
	A. Solid view of model	121
	B. Center-cross section of 3D numerical mesh with 0.4 μm cubical Yee cell dimension.	121
Figure 5.7	Depicted in the time and frequency domain are the Gaussian pulses used in the XFDTD model	
	A. The short excitation pulse has a pulse width equal to 0.348 of the dielectric relaxation time constant for cytoplasm in a chromaffin cell	123
	B. The long excitation pulse width is 4.177 dielectric relaxation time constants.	123
Figure 5.8	The transient EMF spatial distribution surrounding and within a chromaffin cell for a Gaussian pulse plane wave applied to the single cell model for	

	A. a short pulse width	125
	B. a long pulse width. For the short pulse, the time to its maximum is 1.955 picoseconds after the start of the simulation; whereas for the long pulse, the time to its maximum is 22.25 picoseconds into the simulation	126
Figure 5.9	The transient EMF time history surrounding and within a chromaffin cell at the points depicted in Figure 5.2b. A short Gaussian pulse plane wave is applied to the single cell model. The pulse width is 1.733 picoseconds.	127
Figure 5.10	The transient EMF time history surrounding and within a chromaffin cell at the points depicted in Figure 5.1b. A long Gaussian pulse plane wave is applied to the single cell model. The pulse width is 20.8 picoseconds.	127
Figure 5.11	A. Spectral distribution of the transient EMF time history within the cytoplasm at the cell membrane caused by the short pulse	128
Figure 5.12	A. Spectral distribution of the transient EMF time history within the cytoplasm at the cell membrane caused by the long pulse	128
Figure 5.13	The transient \vec{E} field spatial distribution surrounding and within a chromaffin cell cluster excited by a long Gaussian pulse plane wave.	130
Figure 5.14	The transient \vec{E} field time history surrounding and within a cluster of three chromaffin cells at the points depicted in Figure 6b. A long Gaussian pulse plane wave is applied to the cell cluster model. The pulse width is 20.8 picoseconds.	130

Figure 5.15 The fast Fourier transform of the transient \vec{E} field time history surrounding and within a cluster of three chromaffin cells at the points depicted on Figure 6b

131

List of Tables

Table I	Cell Perfusion Chamber parts and their dielectric properties	26
Table II	Comparison Between Field Magnitudes Predicted By The XFDTD Model And Those Calculated From Forward (F) And Reflected (R) Powers At 1 GHz	28
Table III	Referenced and Derived Dielectric Properties	117